ACS APPLIED MATERIALS & INTERFACES

Research Article

www.acsami.org

PEGylated Polyethylenimine as Enhanced T_1 Contrast Agent for Efficient Magnetic Resonance Imaging

Shengyuan Zhou,[†] Zhenkai Wu,[‡] Xiongsheng Chen,[†] Lianshun Jia,[†] and Wei Zhu*[,†]

[†]Department of Orthopedics, Changzheng Hospital, Second Military Medical University, Shanghai 200003, People's Republic of China

[‡]Department of Pediatric Orthopedics, Xinhua Hospital, Shanghai Jiaotong University School of Medicine, Shanghai 200092, People's Republic of China

Supporting Information

ABSTRACT: Currently used small molecular magnetic resonance (MR) imaging contrast agents (CAs) in clinics have relatively short half-lives, which has limited the acquisition of high-resolution organ and angiographic images. Therefore, development of a facile strategy for the synthesis of long-circulating CAs with the transforming potential for MR imaging still remains a great challenge. Here we communicate the design and synthesis of PEGylated polyethylenimine (PEI) and its application as enhanced T_1 CA for the long-circulating blood pool as well as efficient organ and tumor imaging. In this study, PEI was covalently grafted with gadolinium (Gd^{III}) chelator and *m*PEG-NHS, followed by acetylation of the remaining amines to improve biocompatibility and prolong circulation time. With the relatively long circulation time (3.8 h), the formed multifunctional PEI (PEI.NHAc-DTPA(Gd^{III})-*m*PEG) can be used as an enhanced T_1 CA for blood pool and major organ imaging, and could be cleared from the body 96 h post administration through the urinary system. Importantly, the PEI.NHAc-DTPA(Gd^{III})-*m*PEG complexes displayed a strong T_1 contrast effect for tumor imaging through the enhanced permeation and retention effect. These findings suggest that the synthesized PEI.NHAc-DTPA(Gd^{III})-*m*PEG may be used as a promising CA for T_1 MR imaging of various biological systems.

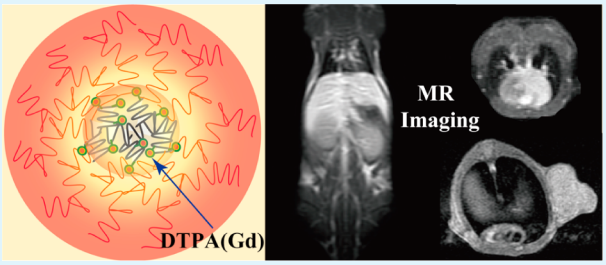

KEYWORDS: *polyethylenimine, PEGylation, gadolinium, MR imaging, tumor imaging*

1. INTRODUCTION

Among various molecular imaging modalities, magnetic resonance (MR) imaging has been used as one of the most powerful tools in clinical noninvasive diagnosis due to its high spatiotemporal resolution and impressive tissue penetration.[1−4] Apart from the instrument and different imaging methodology, the performance of MR imaging is strongly determined by contrast agents (CAs), which could significantly enhance the contrast effect and increase the sensitivity of the images for more accurate clinical diagnosis.[5,6] Based on different models of relaxation, MR imaging CAs could be divided into longitudinal (T_1)-positive agents and transverse (T_2)-negative agents, which respectively lead to brighter image in T_1-weighted MR imaging and darker image in T_2-weighted MR imaging compared with precontrast images.[6] Generally, gadolinium (Gd^{III})- or manganese (Mn^{II})-based CAs[7−9] and superparamagnetic iron oxide nanoparticle-based CAs[5,10−12] are typical T_1 and T_2 contrast materials, respectively. Compared with T_2 CAs which can intrinsically produce dark signals and confuse their location with the signals from bleeding, calcification, tissue−air interfaces, and susceptibility artifacts, T_1-based agents have predominant positive signal-enhancing ability to generate higher spacial resolution.[13] In this case, the current clinically used MR imaging CAs are dominant with paramagnetic Gd^{III}-based complexes, such as Magnevist (Gd-DTPA), Dotarem (Gd-DTOA), and Gadovist (Gd-DO3A-Butriol).[14] Unfortunately, these Gd^{III}-based T_1 CAs are based on small molecular agents, which display severe disadvantages such as short half-decay time and rapid extravasation from the vascular space. Therefore, the contrast enhanced time window for MR imaging is very narrow, which has limited the acquisition of the higher resolution images of angiography as well as organs.[15]

In order to overcome such drawbacks inherent to small molecular CAs, numerous Gd^{III}-loaded macromolecular CAs have been constructed to increase their blood circulation time as well as to improve their imaging specificity.[16] These macromolecular CAs have been developed by simply coupling Gd^{III} chelate to polymers,[9,17] dendrimers,[18,19] micelles,[20] liposomes,[21] and proteins.[22,23] Although these formed agents have demonstrated increased circulation time as well as enhanced MR contrast effect with the dramatically increased Gd^{III} loading, their translation to clinical applications has often been hampered by their sophisticated synthesis, expensive carriers, and difficulty synthesizing large amounts. Therefore,

Received: April 7, 2014
Accepted: July 1, 2014
Published: July 1, 2014

   dx.doi.org/10.1021/am5020875 | ACS Appl. Mater. Interfaces 2014, 6, 11459−11469

Scheme 1. Schematic Illustration of the Design (a) and Synthesis Procedure (b) for Multifunctional PEI for MR Imaging

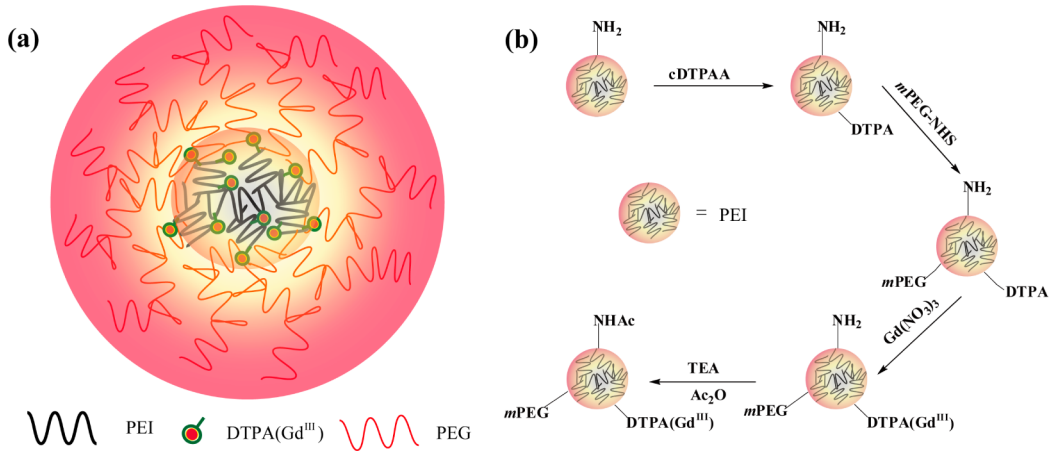

development of a facile strategy for synthesis of Gd^{III}-loaded macromolecular MR imaging CAs with the transforming potential for biomedical imaging still remains a great challenge.

Polyethylenimine (PEI) is an inexpensive reagent and widely available in large quantities, and has been frequently employed as an effective nonviral vector for gene delivery.[24−26] Taking advantage of the high density of amines in its structure, PEI has also been employed as stabilizer or template to synthesize, modify, or assemble inorganic nanomaterials.[27,28] Although amine-rich groups make PEI distinctly cytotoxic,[29,30] a variety of chemical modifications, such as acetylation and PEGylation,[31−33] can address some of these concerns and improve its biocompatibility. Moreover, these amine groups of the PEI endow it to be further modified easily with various desirable functional groups, such as targeting ligands and drug molecules, for targeted drug and gene delivery.[34,35] In our previous work,[36] PEI-mediated multifunctional multiwalled carbon nanotubes (MWCNT) were formed and used for enhanced blood pool and passive tumor MR imaging. However, for further transferring the results obtained with mice to human, the potential biotoxicity of MWCNT should be considered. These studies lead us to hypothesize that PEI itself can also be used as the desired platform for T_1-based MR imaging with the transforming potential.

In this study, multifunctional PEI-loaded Gd^{III} was designed and synthesized for the MR imaging application (Scheme 1a). PEI was first modified with Gd^{III} chelator and polyethylene glycol (PEG). The macromolecules formed were chelated with Gd^{III}, followed by complete acetylation of the remaining PEI amines (Scheme 1b). The obtained PEI.NHAc-DTPA(Gd^{III})-*m*PEG was thoroughly characterized via different techniques and its MR imaging performance was evaluated both in vitro and in vivo. Results show that the multifunctional PEI formed could be used as enhanced T_1 CA for blood pool and major organ imaging. Moreover, this longer blood circulating T_1 contrast effect provides great opportunity for imaging tumors through the enhanced permeation and retention (EPR) effect. Importantly, the facile synthesis and nontoxic property of the polymers used make it the desired platform for MR imaging with the transforming potential.

2. EXPERIMENTAL SECTION

2.1. Materials. Branched polyethylenimine (PEI) (M_w = 25 000), cyclic diethylenetriamine pentaacetic anhydride (cDTPAA), and 3-(4,5-dimethylthiazol-2-yl)-2,5-diphenyltetrazolium bromide (MTT) were purchased from Sigma-Aldrich (St. Louis, Missouri) and used as received. PEG monomethyl ether with one end of *N*-hydroxy succinimidyl ester group (*m*PEG-NHS, M_w = 5000) was obtained from Shanghai Seebio Biotech, Inc. (Shanghai, China). Roswell Park Memorial Institute-1640 (RPMI-1640) medium, fetal bovine serum (FBS), Dulbecco's modified eagle's medium (DMEM), penicillin, and streptomycin were purchased from HyClone Lab., Inc.(Logan, UT). Human epithelial carcinoma (KB) cells and mouse macrophage (Raw 264.7) cells were obtained from the Institute of Biochemistry and Cell Biology (Shanghai, China). Triethylamine (TEA), acetic anhydride (Ac_2O), $GdCl_3$, and all other chemicals were from Sinopharm Chemical Reagent Co., Ltd. (Shanghai, China) and used as received. Regenerated cellulose dialysis membranes (molecular weight cutoff 8000−14 000) were acquired from Shanghai Yuanye Biotechnology Co., Ltd. (Shanghai, China).

2.2. Synthesis of PEI-DTPA. First, 80.0 mg PEI (0.0032 mmol) was dissolved in 40 mL water. Then, 57.1 mg cDTPAA (0.16 mmol) in 6 mL water was added into the solution of PEI under vigorous magnetic stirring. The reaction was continued for 12 h to obtain PEI-DTPA. Finally, the excess reactants were removed from the reaction mixture by extensive dialysis against phosphate buffer solution (PBS) and water for 2 days, followed by lyophilization to obtain the PEI-DTPA.

2.3. Synthesis of PEI.NHAc-DTPA(Gd^{III})-*m*PEG. PEI-DTPA (68.6 mg, 0.0016 mmol) dissolved in 15 mL water was added to 16 mL *m*PEG-NHS solution (160 mg, 0.032 mmol). After 15 h reaction under vigorous magnetic stirring, the reaction solution was purified and lyophilized according to the procedure used for purification of PEI-DTPA to obtain PEI-DTPA-*m*PEG.

For synthesis of PEI.NHAc-DTPA(Gd^{III})-*m*PEG, PEI-DTPA-*m*PEG (114.3 mg, 0.0008 mmol) dissolved in 20 mL water was added to 4 mL $GdCl_3$ (10.5 mg, 0.04 mmol) under vigorous magnetic stirring. Three hours later, TEA (60.0 μL) was added and thoroughly mixed with the reaction mixture for 30 min, and then excess Ac_2O (40.0 μL) was dropwise added into the reaction mixture under vigorous stirring for 18 h to neutralize the remaining PEI amines. The formed PEI.NHAc-DTPA(Gd^{III})-*m*PEG was purified and lyophilized. The control complexes PEI-DTPA(Gd^{III}), PEI.NHAc-DTPA(Gd^{III}), PEI-DTPA(Gd^{III})-*m*PEG, and PEI.NHAc-DTPA-*m*PEG were also synthesized using the same method.

2.4. Characterization Techniques. ^{1}H NMR spectra were measured by a nuclear magnetic resonance spectrometer (Bruker DRX 400, Germany). The Gd^{III} composition of the samples was acquired with Leeman Prodigy inductively coupled plasma-optical emission spectroscopy (ICP-OES, USA). Zeta-potential values of the formed materials were determined by a Zetasizer Nano ZS system (Malvern, UK). UV−vis spectroscopy measurements were conducted by using PerkinElmer (Lambda EZ-210) in transmission mode.

2.5. In Vitro MR Imaging. In vitro T_1-weighted MR images and T_1 relativities were measured with a conventional spin−echo

acquisition in a 3.0 T clinical MR system (GE Medical Systems, USA) at room temperature. Water solution of Gd-DTPA (Magnevist) and the PEI.NHAc-DTPA(Gd^{III})-*m*PEG (1.8 mL) formed with different Gd^{III} molar concentrations (0.1, 0.2, 0.4, 0.6, 0.8, and 1.0 mM) were prepared in 2.0 mL tubes. T_1 relaxation was obtained using the SE/2D sequence and four echoes were employed with the following parameters: FOV = 12 cm, matrix = 256 × 256, TE = 10.7 ms, and TR = 300, 600, 900, 1200 ms.

2.6. In Vitro Cytotoxicity Assay. KB cells were cultured in a 37 °C incubator with 5% CO_2 in RPMI 1640 cell culture medium supplemented with 100 μg/mL streptomycin, 100 U/mL penicillin, and 10% FBS. The cytotoxicity of the materials formed was quantified using MTT reduction assays. In a typical procedure, KB cells were cultured in 96-well plates at a density of approximately 6000 per well overnight to allow the cells to attach. Subsequently, the medium containing PEI-DTPA(Gd^{III}), PEI-DTPA(Gd^{III})-*m*PEG, PEI.NHAc-DTPA(Gd^{III}), and PEI.NHAc-DTPA(Gd^{III})-*m*PEG at the same Gd^{III} molar concentrations (0, 10, 25, 50, 100 μM, respectively) was added. About 24 h later, 20 μL 5 mg/mL MTT solution was added and the cell viability was measured at 570 nm by a Thermo Scientific Multiskan MK3 ELISA reader (USA). After treatment with the PEI.NHAc-DTPA(Gd^{III})-*m*PEG at different Gd^{III} molar concentrations for 24 h, the cell morphology was observed using an inverted phase contrast microscope (Leica DM IL LED) at a magnification of 200× for each sample.

2.7. In Vitro Macrophage Cellular Uptake. To evaluate the macrophage cellular uptake of the materials formed, Raw 264.7 cells were selected and continuously cultured with DMEM supplemented with 10% FBS, streptomycin (100 μg/mL), and penicillin (100 U/mL). About 2×10^6 cells were seeded into each well of 12-well plates before the experiments to bring the cells to confluence. The next day, fresh medium containing PEI-DTPA(Gd^{III}), PEI.NHAc-DTPA(Gd^{III}), PEI-DTPA(Gd^{III})-*m*PEG, and PEI.NHAc-DTPA(Gd^{III})-*m*PEG with the same Gd concentration of 50 μM was separately added and incubated for 4 h. After that, the cell medium in wells was removed, and the cells were washed with PBS buffer 3 times, trypsinsized, and suspended in cell medium. After determining the cell concentrations by hemacytometry, the cells were centrifuged (3000 rpm, 5 min) and digested in aqua regia solution. Finally, the macrophage cellular Gd uptake was determined by ICP-OES.

2.8. Hemolysis Assay. For hemolysis study, fresh human blood stabilized with citrate was provided by Changzheng Hospital (Shanghai, China) and healthy red blood cells were collected according to the procedures reported in the literature.[28,37] Briefly, 1 mL fresh blood was centrifuged to get the isolated red blood cells (2000 rpm, 5 min). Following 4× washing with 6 mL sterile isotonic PBS, 0.3 mL aliquots of the red blood cells were diluted with 2.7 mL PBS. Thereafter, 0.1 mL aliquots of the diluted cell suspension were added to 1.5 mL tubes prefilled with 0.9 mL deionized water (positive control), 0.9 mL PBS (negative control), and 0.9 mL PBS containing PEI.NHAc-DTPA(Gd^{III}) and PEI.NHAc-DTPA(Gd^{III})-*m*PEG with different concentrations (50, 100, 200, and 400 μg/mL), respectively. After gentle shaking, the mixtures were left to stand for 2 h at room temperature, followed by centrifugation at 10 000 rpm for 1 min. Afterward, the photos of the mixtures were taken and the absorbance of the supernatants was recorded by UV−vis spectrophotometer. The hemolysis percentages of the samples were calculated according to the following equation:

$$\text{Hemolysis percentage} = (A_s - A_{nc})/(A_{pc} - A_{nc}) \times 100\% \quad (1)$$

where A_s is the absorbance value of the samples at 541 nm, A_{nc} and A_{pc} are the absorbance values of the negative and positive controls at 541 nm, respectively.

2.9. Blood Circulation and Pharmacokinetics. For in vivo blood circulation and pharmacokinetics, 0.15 mL PEI.NHAc-DTPA-(Gd^{III})-*m*PEG or PEI.NHAc-DTPA(Gd^{III}) saline solution (with Gd^{III} molar concentration 20.0 mM) was administered intravenously in ICR mice. After 0.5, 1, 2, 4, 8, 12, 24, and 36 h post-injection, the blood drawn from eyeballs of mice was harvested. The collected blood samples were weighed and digested in aqua regia solution overnight, and then the Gd^{III} content in the samples was determined by ICP-OES. The remainder of materials formed in the blood was calculated by quantifying the content of Gd^{III}.

2.10. In Vivo Toxicity Studies. All the animal studies were carried out according to the standard protocol approved by the institutional committee for animal care. For in vivo toxicity studies, the male 5-week-old ICR mice weighing about 25 g purchased from Shanghai SLAC Laboratory Animal Co. Ltd. (Shanghai, China) were used. The body weight of ICR mice in both the test group and control group (n = 6 for each group) was recorded for one month after administration. For the test group, 0.15 mL PEI.NHAc-DTPA(Gd^{III})-*m*PEG (with Gd^{III} molar concentration 20.0 mM) saline solution was injected via the tail vein. ICR mice with injection of 0.15 mL saline solution were selected as the control group.

2.11. Histology Analysis. In terms of histology studies, the above ICR mice were sacrificed for one month after administration, and major organs (heart, liver, spleen, lung, and kidneys) were harvested from both control and test groups. Subsequently, the collected tissues were fixed in 10% neutral buffered formalin, embedded in paraffin, and sectioned at 4 μm thickness, followed by staining with hematoxylin and eosin (H&E). Finally, the histological sections were observed by an inverted phase contrast microscope.

2.12. In Vivo Blood Pool and Major Organ MR Imaging. For in vivo blood pool MR imaging, ICR mice were first anesthetized through intraperitoneal injection of pentobarbital sodium. After that, 0.15 mL PEI.NHAc-DTPA(Gd^{III})-*m*PEG (with Gd^{III} molar concentration 20.0 mM) saline solution was intravenously administrated. The T_1-weighted images were performed using a 3.0 T clinical MR system (GE Medical Systems, USA) with 2 mm slice thickness, 6 × 6 cm FOV, and TR/TE 2000/81.9 ms. Two-dimensional spin−echo MR images were obtained before and after administration of the materials at different time points (0.5, 1.5, 3, and 12 h). The total acquisition time was 2.2 min.

2.13. In Vivo Biodistribution. For in vivo biodistribution studies, the ICR mice were intravenously injected with 0.15 mL PEI.NHAc-DTPA(Gd^{III})-*m*PEG saline solution (with Gd^{III} molar concentration 20.0 mM). At different time points post-injection (0.5, 2, 12, 24, 48, and 96 h), the mice were euthanized. Major organs, including heart, liver, spleen, lung, and kidney, were harvested, weighed, and digested in aqua regia solution overnight. For the excretion study, feces and urine (about 0.15 g) were collected at different time points post-injection (0.5, 2, 4, 8, 24, and 48 h) and digested in aqua regia solution overnight. The Gd^{III} content was measured by ICP-OES.

2.14. Blood Analysis. For serum biochemistry assay, 5 healthy ICR mice were intravenously injected with 0.15 mL PEI.NHAc-DTPA(Gd^{III})-*m*PEG saline solution (with Gd^{III} molar concentration 20.0 mM) and sacrificed at 4 days post-injection. In the same time, another 5 healthy ICR mice were used as a control group and sacrificed at 4 days post-injection of 0.15 mL saline solution. The blood drawn from eyeballs of mice was harvested and serum biochemistry parameters including alkaline phosphatase (ALP), alanine aminotransferase (ALT), aspartate aminotransferase (AST), and blood urea nitrogen levels (BUN) were analyzed using an automatic biochemical analyzer (Beckman Coulter Unicel DxC 800).

2.15. In Vivo Tumor MR Imaging. For in vivo tumor MR imaging, the male 6-week-old Balb/c nude mice weighing about 25 g purchased from Shanghai SLAC Laboratory Animal Co. Ltd. were used. A subcutaneous syngenetic transplantable KB xenograft model was established by injecting 5×10^6 KB cells in 0.15 mL saline solution at the right side oxter of the mice. When the tumor nodules had reached a volume of 0.4−0.8 cm^3, PEI.NHAc-DTPA(Gd^{III})-*m*PEG (0.15 mL in saline solution, with Gd^{III} molar concentration 20.0 mM) was injected through the tail vein. Two-dimensional spin−echo MR images were acquired before and 1, 3, and 6 h post- injection. The MR images were processed using a similar strategy to that described above for blood pool and major organ MR imaging studies.

2.16. Statistical Analysis. All data were expressed in this article as mean ± standard deviation (SD). One-way ANOVA statistical analysis was performed by using Origin 8.0 software to evaluate the significance

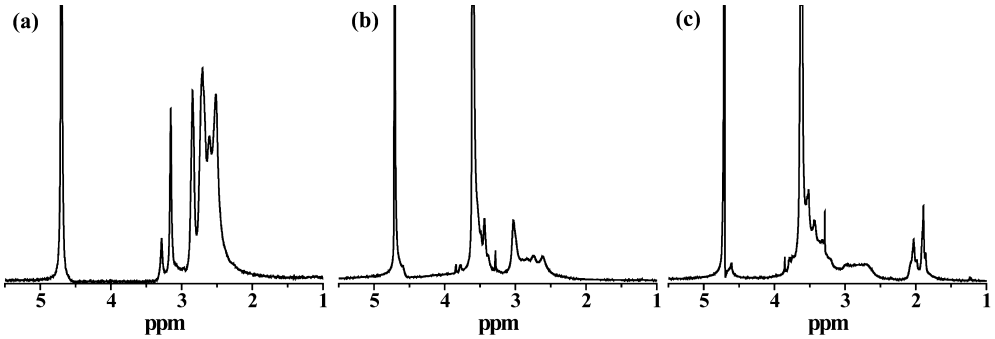

Figure 1. ^{1}H NMR spectra of PEI-DTPA (a), PEI-DTPA-*m*PEG (b), and PEI.NHAc-DTPA-*m*PEG (c) dispersed in D_2O.

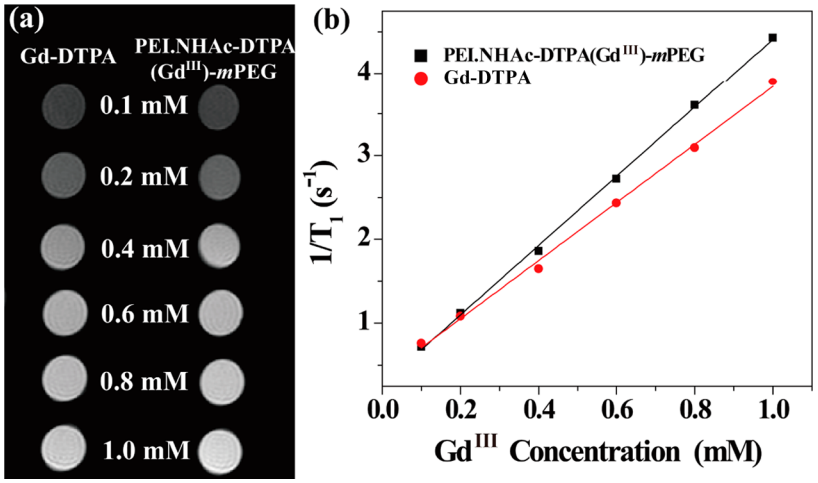

Figure 2. T_1 MR images (a) and linear fitting of r_1 (b) of Gd-DTPA and PEI.NHAc-DTPA(Gd^{III})-*m*PEG as a function of Gd^{III} molar concentration.

of the experimental data. 0.05 was selected as the significance level, and the data were indicated with (*) for $p < 0.05$, (**) for $p < 0.01$, and (***) for $p < 0.001$, respectively.

3. RESULTS AND DISCUSSION

3.1. Synthesis and Characterization of PEI.NHAc-DTPA(Gd^{III})-*m*PEG. To prove our hypothesis that covalent functionalized PEI-based macromolecules enable longer circulation times for effective in vivo T_1 MR imaging applications, we were able to generate PEGylated PEI-based macromolecules for T_1 MR imaging (Scheme 1). Through covalent functionalization, the macromolecules formed were able to show better biocompatibility, longer circulation time, and excellent in vivo blood pool, organ, and passive tumor MR imaging.

To enable MR imaging, PEI was first covalently modified with the Gd^{III} chelator cDTPAA, and the PEI-DTPA formed was detected by ^{1}H NMR spectroscopy. In the ^{1}H NMR spectrum of PEI-DTPA (Figure 1a), the peaks between 2.1 and 3.0 ppm are related to the $-CH_2-$ proton signals of PEI,[38] while the chemical shift at 3.2 and 3.4 ppm is associate with the $-CH_2-$ proton peaks of DTPA. The number of DTPA per PEI was calculated to be 48.7 ± 1.5 based on four batches of PEI-DTPA, which is consistent with the theoretical value of 50 because of the initial molar feeding ratio of cDTPAA and PEI. In addition, the zeta potential of PEI and PEI-DTPA was measured to confirm the surface modification (Table S1, Supporting Information). It is clear that the positive surface potential of PEI (48.42 ± 6.96 mV) decreased to 35.46 ± 10.21 mV after the cDTPAA modification. It is notable that the zeta potential increased dramatically to 52.59 ± 7.28 mV after the Gd^{III} chelation.

Surface PEGylation of nanoparticles is demonstrated to be the most preferred and effective method for improving biocompatibility, avoiding clearance of NPs by the reticuloendothelial system (RES), and increasing circulation time.[39−41] Therefore, PEGylation of the PEI-DTPA amines was performed. As shown in Figure 1b, compared with the ^{1}H NMR spectrum of the PEI-DTPA, that of PEI-DTPA-*m*PEG shows additional peaks at 3.5 and 3.2 ppm, which are related to ethylene backbone and methoxyl protons of PEG, respectively. The number of *m*PEG per PEI was calculated to be 19.2 ± 0.7 (based on four batches of samples), in accordance with the theoretical value of 20 due to the initial molar feeding ratio of *m*PEG-NHS and PEI-DTPA. After further acetylation, the chemical shifts at 1.7−1.9 and 1.9−2.1 ppm are associated with the acetyl proton signals linked with the secondary and tertiary amines, respectively (Figure 1c).[38] These results verify the successful PEGylation and acetylation of PEI-DTPA.

Due to the covered amine group, PEGylation leads to a significantly decreased surface potential of PEI-DTPA(Gd^{III})-*m*PEG (20.16 ± 5.84 mV) compared with that of PEI-DTPA(Gd^{III}) (Supporting Information Table S1). To further reduce the surface charge, the acetylation of the PEI-DTPA(Gd^{III})-*m*PEG amines was performed and the nearly electroneutral PEI.NHAc-DTPA(Gd^{III})-*m*PEG with zeta potential of 3.98 ± 1.62 mV was obtained. It is notable that the acetylated product PEI.NHAc-DTPA(Gd^{III}) without PEGylation also has relatively low zeta potential (5.87 ± 0.79 mV, Supporting Information Table S1), and this will be beneficial

for prolonging its circulation half-life and reducing the long-term toxicity issues. The number of Gd^{III} per complex was measured to be 47.4 ± 2.5 by ICP-OES, which is consistent with the theoretical value (50) based on the initial molar feeding ratio.

The stability of the chelated Gd^{III} in the PEI.NHAc-DTPA-*m*PEG was also inspected by dialyzing 5 mL PEI.NHAc-DTPA(Gd^{III})-*m*PEG solution (8 mg/mL) against PBS. Two weeks later, 3 mL of above PBS outer phase was measured by ICP-OES. The results show that there were no Gd^{III} released from the PEI.NHAc-DTPA(Gd^{III})-*m*PEG, which is essential to reduce the possibility of toxic side effects and the onset of nephrogenic systemic fibrosis induced by free Gd^{III}.

3.2. MR Relaxometry. To investigate the T_1 contrast effect of the formed Gd^{III} loaded multifunctional PEI, in vitro MR imaging was performed. As shown in Figure 2a, similar to the Magnevist (Gd-DTPA), the PEI.NHAc-DTPA(Gd^{III})-*m*PEG displays brighter T_1-weighted MR images with the increase of Gd^{III} molar concentration. To compare the signal enhancement of the materials formed with that of Gd-DTPA, the r_1 relaxivity was calculated by plotting their $1/T_1$ as a function of different Gd^{III} molar concentrations. Results showed that Gd-DTPA and PEI.NHAc-DTPA(Gd^{III})-*m*PEG displayed r_1 values of 3.40 and 4.20 $mM^{-1}\cdot s^{-1}$, respectively, suggesting that the loading of Gd^{III} into multifunctional PEI could slightly increase the r_1 relaxivity and improve the T_1 contrast effect (Figure 2b). It is likely that only marginal increase in r_1 was due to a large amount of internal Gd^{III} motion within the polymers formed caused by the PEG linkers, which has previously been reported for Gd^{III}-conjugated dendrimer nanoclusters.[42] However, based on the r_1 relaxivity per Gd^{III} and the average Gd^{III} content of each PEI, it is calculated that the r_1 relaxivity per PEI was as high as 199 $mM^{-1}\ s^{-1}$. Furthermore, it is reported that future improvements in the r_1 value per particle should be gained through the development of higher Gd^{III}-loaded carriers, since the theoretical maximum r_1 per Gd^{III} was estimated to be only about 80 at 1.5 T.[42] Also, biodegradable materials or linkages should be introduced into the macromolecular gadolinium-based MRI CAs for their effective excretion.[43]

3.3. Cytotoxicity Investigation. Before their usage as a MR imaging CA, it is essential to evaluate the cytocompatibility of the formed complexes. MTT assay was conducted to estimate the KB cell viability treated with PEI-DTPA(Gd^{III}), PEI-DTPA(Gd^{III})-*m*PEG, PEI.NHAc-DTPA(Gd^{III}), and PEI.NHAc-DTPA(Gd^{III})-*m*PEG at different Gd^{III} molar concentrations for 24 h. As shown in Figure 3, PEI-DTPA(Gd^{III}) exhibits cytotoxicity at 10 μM ($p < 0.001$) compared with the KB cells treated with PBS (control cells), due to the high positive charge of PEI. After PEGylation, the cytocompatibility of PEI-DTPA(Gd^{III})-*m*PEG has significantly improved and could not display appreciable cytotoxicity within Gd^{III} molar concentration of 50 μM. Through further acetylation, the PEI.NHAc-DTPA(Gd^{III})-*m*PEG formed did not display any noticeable cytotoxicity at the relatively higher Gd^{III} molar concentration of 100 μM. Also, the product PEI.NHAc-DTPA(Gd^{III}) without PEGylation did not show any noticeable cytotoxicity at the Gd^{III} molar concentration of 100 μM. This improved biocompatibility means the positive surface charge of PEI could be shielded and neutralized via PEGylation and acetylation as shown in Supporting Information Table S1, in agreement with the previous report.[38]

To further confirm the cytocompatibility of PEI.NHAc-DTPA(Gd^{III})-*m*PEG, the KB cell morphology was observed after incubation for 24 h. As displayed in Figure S1 (Supporting Information), cells treated with PEI.NHAc-DTPA(Gd^{III})-*m*PEG at the given concentrations (Figure S1b–e) are fairly healthy and exhibit similar morphology to control cells (Figure S1a). Therefore, these results demonstrated their excellent biocompatibility and the feasibility for further in vivo investigation.

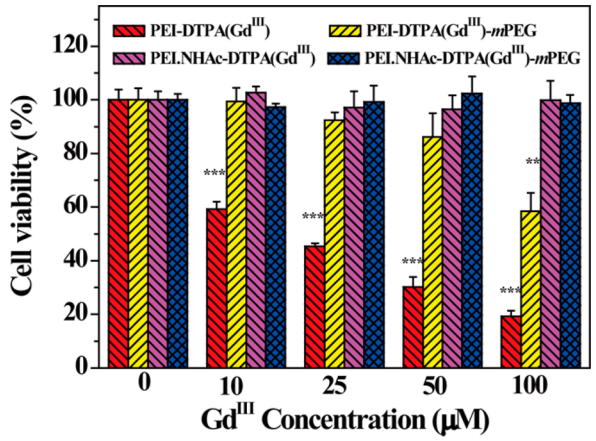

Figure 3. MTT assay of the viability of KB cells after treatment with PEI-DTPA(Gd^{III}), PEI-DTPA(Gd^{III})-*m*PEG, PEI.NHAc-DTPA-(Gd^{III}), and PEI.NHAc-DTPA(Gd^{III})-*m*PEG at the Gd^{III} molar concentrations of 0–100 μM for 24 h.

3.4. Macrophage Uptake of the Formed Materials. For their blood pool imaging applications, the CAs formed should be able to escape the macrophage uptake. Therefore, in this study, RAW 264.7 cells were used as a model of phagocytes to evaluate the in vitro stealth behavior of different modified PEI according to the previous report.[28] ICP-OES was used to quantify the cellular uptake of Gd content after the Raw 264.7 cells were treated with the materials formed for 4 h at the Gd concentration of 50 μM. As shown in Supporting Information Figure S2, the treatment of PEI-DTPA(Gd^{III}) results in a significantly high Gd uptake of 11.3 ± 2.4 pg per cell, while that treated with PEI-DTPA(Gd^{III})-*m*PEG has relatively low Gd uptake of 3.8 ± 1.5 pg per cell. In contrast, the same cells treated with PEI.NHAc-DTPA(Gd^{III}) and PEI.NHAc-DTPA-(Gd^{III})-*m*PEG display much lower Gd uptake of 0.7 ± 0.18 and 0.6 ± 0.14 pg per cell, respectively, in agreement with the previous report.[28] These results suggested that the nearly electroneutral materials with PEGylation and acetylation could effectively reduce their macrophage cellular uptake and promise good stealth properties for in vivo applications.

3.5. Hemolytic Behavior. Blood compatibility is a critical factor for in vivo bioapplications especially for long-circulating CAs. Therefore, the hemolysis experiments were employed to assess the hemocompatibility of the formed materials according to the previous reports.[28,37] As shown in Figure 4, no visible hemolysis effect can be observed visually even at a concentration as high as 400 μg/mL for both PEI.NHAc-DTPA(Gd^{III})-*m*PEG and PEI.NHAc-DTPA(Gd^{III}). To further quantitatively determine the hemolysis effect of the samples, the absorbance of the supernatant at 541 nm (hemoglobin) was measured using UV–vis spectroscopy. The hemolysis percentages of both materials at different concentrations are all less than 2%, which suggests excellent biocompatibility of the materials formed with blood cells and is favorable for their in vivo applications.

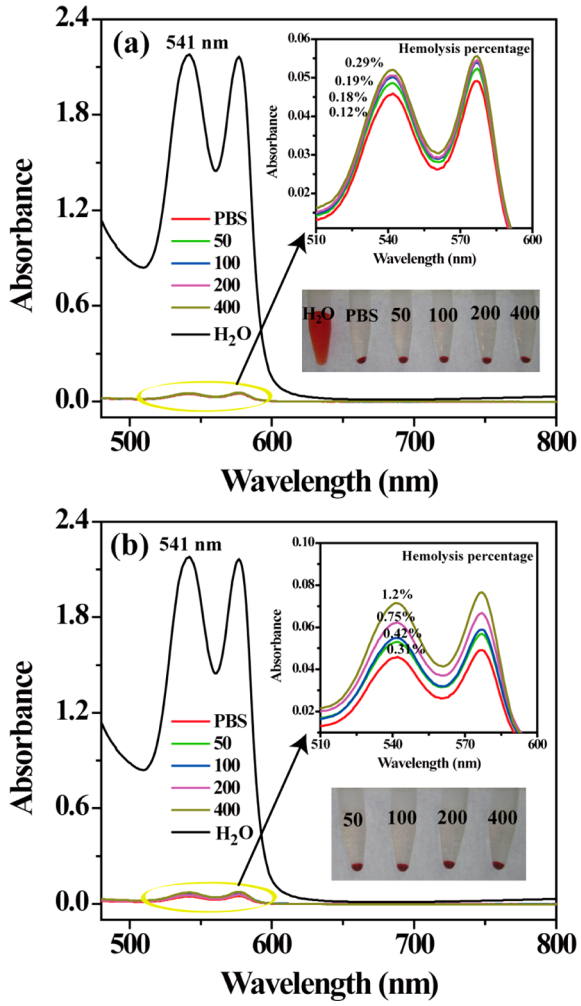

Figure 4. Hemolytical activity of the PEI.NHAc-DTPA(Gd^{III})-*m*PEG (a) and PEI.NHAc-DTPA(Gd^{III}) (b) at different material concentrations (50, 100, 200, and 400 μg/mL, respectively). Water and PBS were used as positive and negative control, respectively. The bottom-right insets show the photograph of centrifuged red blood cells after exposure to water, PBS, and different concentrations of the materials. The upper-right insets show the enlarged UV–vis spectra shown in each panel.

3.6. Pharmacokinetics Study. For efficient blood pool MR imaging in vivo, it is essential to investigate the pharmacokinetics of the materials formed. The Gd^{III} molar concentration in the blood samples of mice after administration was measured by ICP-OES (Figure 5). It is notable that the half-decay time of the PEI.NHAc-DTPA(Gd^{III})-*m*PEG was measured to be 3.8 h, which is nearly 4 times longer than that of the materials PEI.NHAc-DTPA(Gd^{III}) without PEGylation (0.8 h). This relatively longer circulation time of PEI.NHAc-DTPA(Gd^{III})-*m*PEG may be due to the fact that the branch structure of PEI could provide jagged reaction sites for the following PEGylation, and this structure is quite similar to that of highly branched PEG. Also, it is reported that the branched PEG has better performance than the linear one in improving the circulation time.[44] This longer half-decay time is a prerequisite for their application in both blood pool and tumor MR imaging, since the longer the circulation time, the greater the chance for materials to reach tumor tissue via an EPR effect.

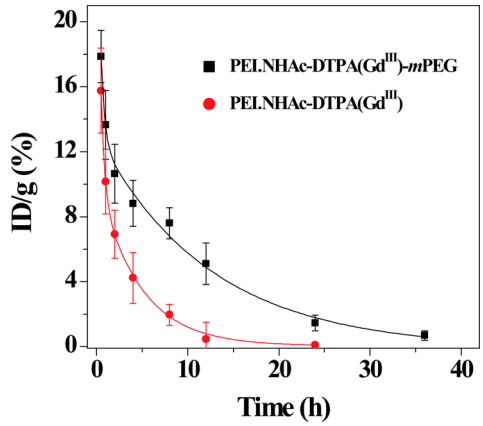

Figure 5. Blood circulation and pharmacokinetic data obtained for PEI.NHAc-DTPA(Gd^{III}) and PEI.NHAc-DTPA(Gd^{III})-*m*PEG.

3.7. In Vivo Toxicology Study. To further investigate the long-term in vivo biosafety of the complexes formed, body weight measurement, behavior observation, as well as histological changes of major organs were used. As shown in Figure S3a (Supporting Information), both the test and control groups display similar body weight increases in the 30-day period, and there was almost no notable difference between these two groups. In addition, the test group does not present any changes in exploratory behavior, activity, drinking, eating, and neurological status compared with the control group during a 30-day period. To continue to determine whether PEI.NHAc-DTPA(Gd^{III})-*m*PEG caused any histopathological abnormalities, histological changes in major organs were analyzed via H&E staining one month after administration. The H&E stained slices of the test group did not show any noticeable lesions, hydropic damage, or any other adverse effect and their organ morphology was as normal as that of the control group (Supporting Information Figure S3b). Based on the results above, PEGylated PEI-based T_1 CA exhibited high biocompatibility and appeared to be more promising for further MR imaging applications.

3.8. Blood Pool MR Imaging. Based on the excellent in vitro T_1 contrast effect and in vivo biocompatibility, as well as longer half-decay time of PEI.NHAc-DTPA(Gd^{III})-*m*PEG, further in vivo blood pool and major organ MR imaging performance was explored. As shown in Figure 6, the brighter regions of postcaval and major organs as pointed by the red arrow can be clearly observed post-injection of the materials. For blood pool MR imaging, the postcaval vein became visible as brighter regions in Figure 6a at 0.5 h post-injection, demonstrating that PEGylated PEI-based CA can enhance T_1 relaxation in the circulating system. Importantly, this contrast enhancement was clearly visible 3 h post-injection. For quantitative analysis of the MR contrast effect, the average MR signal intensities within finely operator-defined regions of interest regions were measured. Then, the relative signal enhancement (RSE) was calculated as the ratio of the signal intensities in the post-injection image and the pre-injection image (Figure 7). The RES of the postcaval were 250 ± 34.8%, 195 ± 23.7%, 135 ± 58.4%, and 110 ± 20.1% at 0.5, 1.5, 3, and 12 h post-administration, which suggest the slow clearance of CA from the bloodstream during circulation. It is notable that the T_1 contrast enhanced time of PEI.NHAc-DTPA(Gd^{III})-*m*PEG is comparable to the reported long-circulating CAs, such as small-sized iron oxide nanoparticles (1 h)[45] and Gd^{III}

dx.doi.org/10.1021/am5020875 | ACS Appl. Mater. Interfaces 2014, 6, 11459–11469

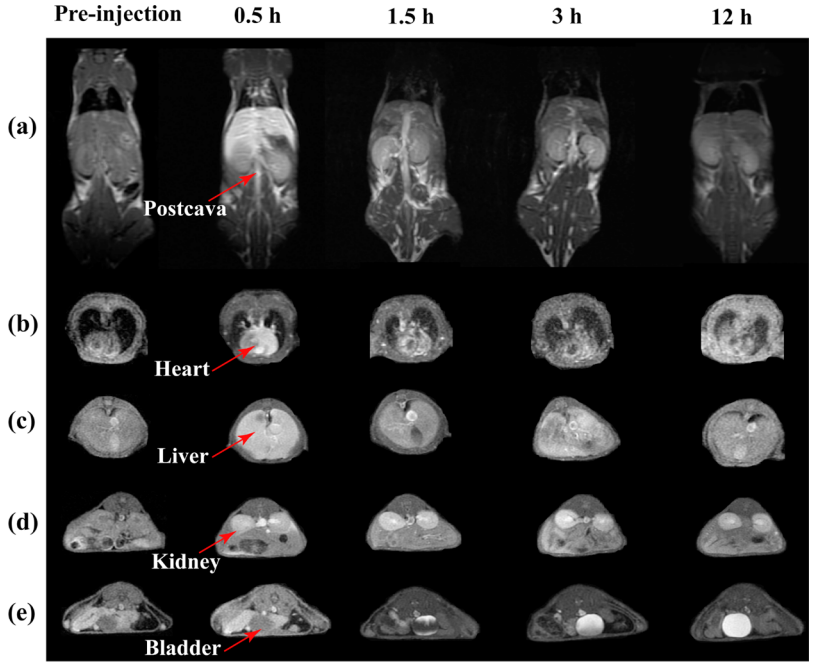

Figure 6. T_1-weighted MR images of a mouse postcaval (a), heart (b), liver (c), kidney (d), and bladder (e) after intravenous injection of PEI.NHAc-DTPA(Gd^{III})-*m*PEG for different times.

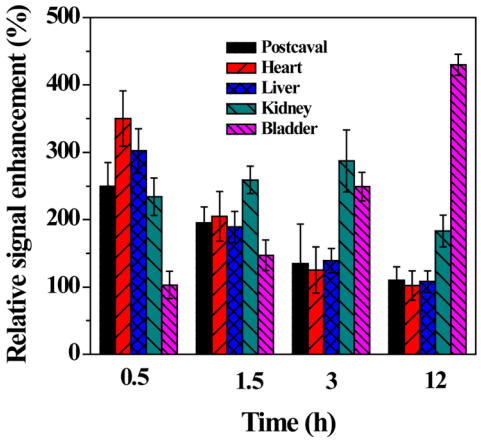

Figure 7. Relative T_1 MR signal enhancement of postcaval, heart, liver, kidney, and bladder of the mouse after intravenous injection of PEI.NHAc-DTPA(Gd^{III})-*m*PEG for different times.

complexes of DTPA-Biphenyl-2,2′-bisamides (2 h).[46] In addition, this long-term blood pool MR imaging is important in clinical diagnosis, since it can be used to detect the thrombosis,[47,48] carotid atherosclerosis,[49] myocardial infarction,[50] pulmonary embolism,[51] kidney hypoxia and fibrosis,[52] atherosclerotic plaque,[53] as well as angiogenesis of tumor.[54] Also, long-term blood pool imaging is essential for steady-state imaging, which needs more time to obtain and can get high-resolution images.[46,55]

3.9. Major Organ MR Imaging. As illustrated in Figure 6b–e, the heart, liver, kidneys, and bladder region became brighter zones with the administration of PEI.NHAc-DTPA-(Gd^{III})-*m*PEG due to its T_1 contrast effect within these organs. To be specific, the contrast effect of the heart can be easily observed post-injection because of the appearance of the CA formed in the blood (Figure 6b). At 0.5 h post-injection, brighter region of the whole heart was clearly visible with RSE of 350 ± 41.3% (Figure 7). After that, the relative heart signal enhancement decreased with time and reached just 102 ± 21.7% 12 h post-injection, because of the gradual elimination of CA from the bloodstream. Similarly, the contrast enhancement of the liver can be visibly monitored post-injection, suggesting that the injected CA is able to enter the liver with the blood circulation (Figure 6c). Again, the RSE of liver decreased considerably from 302 ± 32.9% (0.5 h) to about 108 ± 15.8% (12 h), due to its slow clearance. It is remarkable that the materials could not accumulate in the liver with time because of the reduced uptake by RES. With regard to kidneys, the contrast enhancement can be definitely observed (Figure 6d). Just 0.5 h post-injection, a brighter area with a clearer border for the entire kidneys could be observed with significant RSE of 234 ± 27.9% (Figure 7). The RSE stabilized at about 259 ± 20.1% in the following 3 h and decreased to 183 ± 23.6% 12 h after administration. For the bladder, it is noteworthy that the RSE is still as low as 103 ± 20.3% 0.5 h after administration. Also, the gray bladder imaging marked by the red arrow in Figure 6e indicated the relatively few materials accumulated in the bladder, due to the longer circulation time. Then, the bladder region became brighter and brighter with time and the RSE increased from 147 ± 22.6% to 430 ± 15.8% during the period between 1.5 and 12 h. This means the complexes formed could be excreted out of the body through the urinary system over time. These results indicated that the PEGylated PEI-based MR CA has excellent in vivo behavior, proving the clear major organ MR imaging and easy excretion out of body.

3.10. Biodistribution Study and Blood Examination. For more accurate biodistribution behavior of PEI.NHAc-DTPA(Gd^{III})-*m*PEG in mice, the major organs (heart, liver, spleen, lung, and kidney) of test mice were collected and quantified. As shown in Figure 8, liver and spleen have similar uptake of Gd^{III} with kidney and heart at nearly all time points. This means that the materials formed could effectively reduce the uptake of the RES in liver and spleen compared with many nanomaterials applied in biomedicine, which showed that the

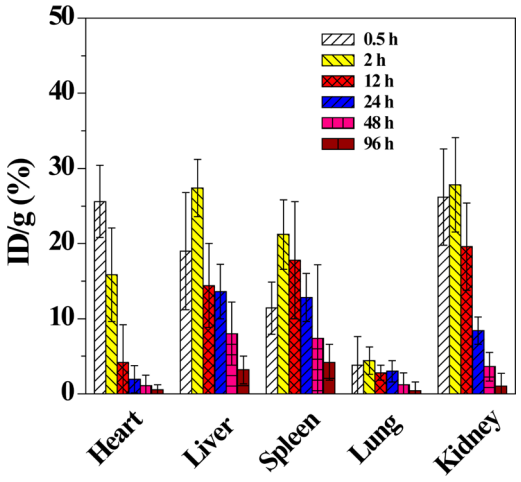

Figure 8. Biodistribution of PEI.NHAc-DTPA(Gd^{III})-*m*PEG in the major organs of the mice including heart, liver, spleen, lung, and kidney.

uptake of materials in liver or spleen was about ten times greater than that in other organs.[19,56] Therefore, it is essential for the CA formed to be excreted out of the body through the urinary system and safely used in clinical application. The content of Gd^{III} in kidney slightly increased from 26.2% to 27.4% injected dose per g (ID/g) in the first 2 h; after that, the figure dips to only 1% ID/g at 96 h post-administration. The Gd^{III} content in heart is relatively high in the first 2 h due to the high Gd^{III} content in the residual blood of heart. Also, this figure displayed a continuous decrease over time because of the decrease of Gd^{III} content in the residual blood, while the Gd^{III} content in lung was relatively low at all time points. It is noteworthy that nearly all the Gd^{III} was cleared from the bodies 96 h after administration, with very little remaining in liver and spleen (ID/g < 4%). To prove the hepatic safety of the materials formed, apart from the H&E staining, the liver function parameters including AST, ALP, and ALT were measured.[57] The results show that all three serum biochemistry parameters (Table S2, Supporting Information) of the test group have similar values to that of the control group (p > 0.05), which indicated good function of the liver.

To further investigate the routes of excretion of the CA formed, the presence of Gd in the urine and feces was also quantitatively analyzed.[58] As shown in Supporting Information Figure S4, the dose of Gd in urine increased sharply at the first 4 h and reached 10.7% ID/g, then this figure was reduced slightly to 9.1% ID/g at 8 h. After that, the dose of Gd in the urine decreased dramatically to 0.8% ID/g 48 h later. In contrast, the dose of Gd in the feces was relatively low (below 0.8% ID/g) at all time points, even though it shows a gradual increase within 24 h. This means that excretion is predominantly through the urinary system, which is consistent with the results obtained from in vivo MR imaging. To prove the renal safety of the materials formed, the BUN level was analyzed. The results (Supporting Information Table S2) show that the BUN level of the test group has a similar value to that of the control group (p > 0.05), suggesting the kidney in good working order.[57]

3.11. In Vivo Tumor MR Imaging. The inspiring long circulation time and excellent in vivo blood pool and major organ MR imaging performance of PEI.NHAc-DTPA(Gd^{III})-*m*PEG drives us to pursue its applicability in tumor MR imaging using a KB xenotransplanted model. The mice were scanned by MR after 1, 3, and 6 h post-injection (Figure 9). In images acquired pre-administration, there was little inherent contrast between tumor tissue and surrounding muscle (Figure 9a). One hour after administration, the subcutaneous tumor appeared brighter than adjacent tissues. After that, the tumor lesion region steadily became clearer with the increase of time and the image shows accurate delineation of the tumor boundary 6 h later, which suggested efficient diffusion of PEI.NHAc-DTPA(Gd^{III})-*m*PEG in the tumor through the EPR effect. Quantitatively, the RSE of the tumor region increased gradually and finally reached 192 ± 13.6% in 6 h as shown in Figure 9b. This excellent tumor MR imaging performance may be due to the relatively long circulating half-life, since the

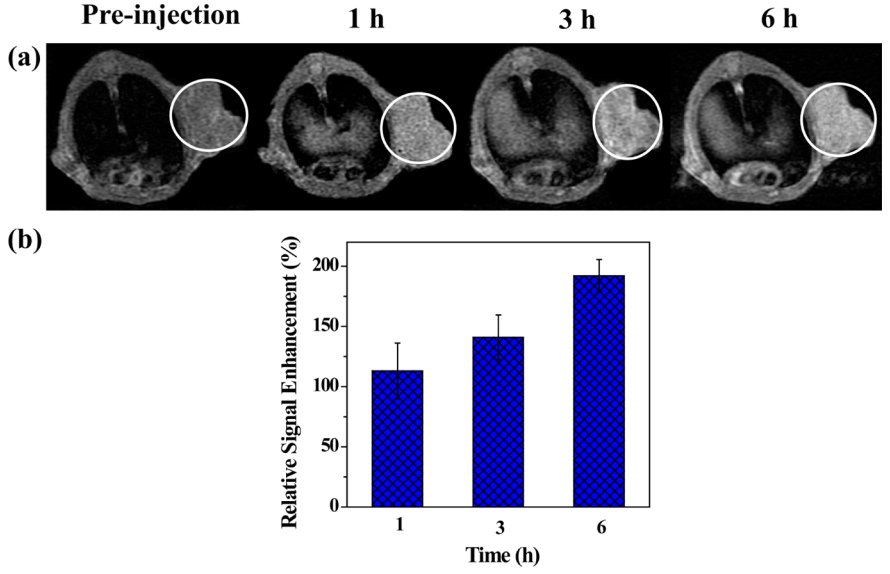

Figure 9. T_1-weighted MR images (a) and the relative T_1 MR signal enhancement (b) of the xenograft KB tumor model before and at different time points after intravenous injection of PEI.NHAc-DTPA(Gd^{III})-*m*PEG.

efficiency of passively targeting a tumor through EPR is highly dependent on blood circulation time.

4. CONCLUSIONS

To conclude, a facile strategy has been developed for the construction of PEGylated PEI-based MR CA for in vivo long-circulating blood pool as well as efficient organ and tumor imaging. The multifunctional PEI formed exhibited good biocompatibility and better MR contrast effect. We showed that they can be used as enhanced T_1 CA for blood pool and major organ imaging, and could be cleared out of the body in living subjects through the urinary system. Moreover, the PEI.NHAc-DTPA(Gd^{III})-*m*PEG developed were useful for passive tumor targeting through the EPR effect, and display a strong T_1 contrast effect for tumor imaging. These results suggest that the synthesized multifunctional PEI may be used as a promising CA for T_1 MR imaging of various biological systems, especially in cancer diagnosis. With the high density of amino groups on the surface, it is expected that functional PEI may be used as a versatile platform for targeted imaging and/or drug and gene delivery for tumor diagnosis and therapy.

■ ASSOCIATED CONTENT

Supporting Information

Zeta potential data, KB cell morphology, macrophage uptake assay, mouse body weight measurement, histological changes study, serum biochemistry assay, and Gd dose in the excreted feces and urine. This material is available free of charge via the Internet at http://pubs.acs.org.

■ AUTHOR INFORMATION

Corresponding Author

*Tel: +86 21 81885637; fax: +86 21 63520020. E-mail: monarch1978@163.com.

Author Contributions

The manuscript was written through contributions of all authors. All authors have given approval to the final version of the manuscript. Shengyuan Zhou and Zhenkai Wu contributed equally to this work.

Notes

The authors declare no competing financial interest.

■ ACKNOWLEDGMENTS

This research is financially supported by the National Natural Science Foundation of China (81201378).

■ REFERENCES

(1) Gao, J.; Liang, G.; Cheung, J. S.; Pan, Y.; Kuang, Y.; Zhao, F.; Zhang, B.; Zhang, X.; Wu, E. X.; Xu, B. Multifunctional Yolk-shell Nanoparticles: A Potential MRI Contrast and Anticancer Agent. *J. Am. Chem. Soc.* **2008**, *130*, 11828−11833.

(2) Logothetis, N. K. What We Can Do and What We Cannot Do with fMRI. *Nature* **2008**, *453*, 869−878.

(3) Marradi, M.; Alcantara, D.; Martinez de la Fuente, J.; Luisa Garcia-Martin, M.; Cerdan, S.; Penades, S. Paramagnetic Gd-based Gold Glyconanoparticles as Probes for MRI: Tuning Relaxivities with Sugars. *Chem. Commun.* **2009**, 3922−3924.

(4) Cheng, L.; Yang, K.; Li, Y.; Chen, J.; Wang, C.; Shao, M.; Lee, S.-T.; Liu, Z. Facile Preparation of Multifunctional Upconversion Nanoprobes for Multimodal Imaging and Dual-Targeted Photothermal Therapy. *Angew. Chem., Int. Ed.* **2011**, *50*, 7385−7390.

(5) Lee, N.; Hyeon, T. Designed Synthesis of Uniformly Sized Iron Oxide Nanoparticles for Efficient Magnetic Resonance Imaging Contrast Agents. *Chem. Soc. Rev.* **2012**, *41*, 2575−2589.

(6) Terreno, E.; Castelli, D. D.; Viale, A.; Aime, S. Challenges for Molecular Magnetic Resonance Imaging. *Chem. Rev.* **2010**, *110*, 3019−3042.

(7) Baek, M. J.; Park, J. Y.; Xu, W.; Kattel, K.; Kim, H. G.; Lee, E. J.; Patel, A. K.; Lee, J. J.; Chang, Y.; Kim, T. J.; Bae, J. E.; Chae, K. S.; Lee, G. H. Water-Soluble MnO Nanocolloid for a Molecular T_1 MR Imaging: A Facile One-Pot Synthesis, In Vivo T_1 MR Images, and Account for Relaxivities. *ACS Appl. Mater. Interfaces* **2010**, *2*, 2949−2955.

(8) Zhang, M.; Cao, Y.; Chong, Y.; Ma, Y.; Zhang, H.; Deng, Z.; Hu, C.; Zhang, Z. Graphene Oxide Based Theranostic Platform for T1-Weighted Magnetic Resonance Imaging and Drug Delivery. *ACS Appl. Mater. Interfaces* **2013**, *5*, 13325−13332.

(9) Xu, Q.; Zhu, L.; Yu, M.; Feng, F.; An, L.; Xing, C.; Wang, S. Gadolinium(III) Chelated Conjugated Polymer as a Potential MRI Contrast Agent. *Polymer* **2010**, *51*, 1336−1340.

(10) Lee, N.; Choi, Y.; Lee, Y.; Park, M.; Moon, W. K.; Choi, S. H.; Hyeon, T. Water-Dispersible Ferrimagnetic Iron Oxide Nanocubes with Extremely High r2 Relaxivity for Highly Sensitive In Vivo MRI of Tumors. *Nano Lett.* **2012**, *12*, 3127−3131.

(11) Shi, X.; Wang, S. H.; Swanson, S. D.; Ge, S.; Cao, Z.; Van Antwerp, M. E.; Landmark, K. J.; Baker, J. R., Jr. Dendrimer-Functionalized Shell-Crosslinked Iron Oxide Nanoparticles for In Vivo Magnetic Resonance Imaging of Tumors. *Adv. Mater.* **2008**, *20*, 1671−1678.

(12) Yang, H.; Zhuang, Y.; Hu, H.; Du, X.; Zhang, C.; Shi, X.; Wu, H.; Yang, S. Silica-Coated Manganese Oxide Nanoparticles as a Platform for Targeted Magnetic Resonance and Fluorescence Imaging of Cancer Cells. *Adv. Funct. Mater.* **2010**, *20*, 1733−1741.

(13) Na, H. B.; Hyeon, T. Nanostructured T_1 MRI Contrast Agents. *J. Mater. Chem.* **2009**, *19*, 6267−6273.

(14) Liu, Y.; Zhang, N. Gadolinium Loaded Nanoparticles in Theranostic Magnetic Resonance Imaging. *Biomaterials* **2012**, *33*, 5363−5375.

(15) Lee, G. H.; Chang, Y.; Kim, T.-J. Blood-Pool and Targeting MRI Contrast Agents: From Gd-Chelates to Gd-Nanoparticles. *Eur. J. Inorg. Chem.* **2012**, *2012*, 1924−1933.

(16) L. Villaraza, A. J.; Bumb, A.; Brechbiel, M. W. Macromolecules, Dendrimers, and Nanomaterials in Magnetic Resonance Imaging: The Interplay Between Size, Function, and Pharmacokinetics. *Chem. Rev.* **2010**, *110*, 2921−2959.

(17) Liu, Y.; Chen, Z.; Liu, C.; Yu, D.; Lu, Z.; Zhang, N. Gadolinium-Loaded Polymeric Nanoparticles Modified with Anti-VEGF as Multifunctional MRI Contrast Agents for the Diagnosis of Liver Cancer. *Biomaterials* **2011**, *32*, 5167−5176.

(18) Han, L.; Li, J.; Huang, S.; Huang, R.; Liu, S.; Hu, X.; Yi, P.; Shan, D.; Wang, X.; Lei, H.; Jiang, C. Peptide-Conjugated Polyamidoamine Dendrimer as a Nanoscale Tumor-targeted T_1 Magnetic Resonance Imaging Contrast Agent. *Biomaterials* **2011**, *32*, 2989−2998.

(19) Wen, S.; Li, K.; Cai, H.; Chen, Q.; Shen, M.; Huang, Y.; Peng, C.; Hou, W.; Zhu, M.; Zhang, G.; Shi, X. Multifunctional Dendrimer-Entrapped Gold Nanoparticles for Dual Mode CT/MR Imaging Applications. *Biomaterials* **2013**, *34*, 1570−1580.

(20) Grogna, M.; Cloots, R.; Luxen, A.; Jerome, C.; Passirani, C.; Lautram, N.; Desreux, J.-F.; Detrembleur, C. Polymer Micelles Decorated by Gadolinium Complexes as MRI Blood Contrast Agents: Design, Synthesis and Properties. *Polym. Chem.* **2010**, *1*, 1485−1490.

(21) de Smet, M.; Langereis, S.; van den Bosch, S.; Bitter, K.; Hijnen, N. M.; Heijman, E.; Grüll, H. SPECT/CT Imaging of Temperature-Sensitive Liposomes for MR-Image Guided Drug Delivery with High Intensity Focused Ultrasound. *J. Controlled Release* **2013**, *169*, 82−90.

(22) Kim, J. H.; Astary, G. W.; Nobrega, T. L.; Kantorovich, S.; Carney, P. R.; Mareci, T. H.; Sarntinoranont, M. Dynamic Contrast-Enhanced MRI of Gd-Albumin Delivery to the Rat Hippocampus In

Vivo by Convection-Enhanced Delivery. *J. Neurosci. Methods* **2012**, *209*, 62−73.
(23) Nwe, K.; Milenic, D.; Bryant, L. H.; Regino, C. A. S.; Brechbiel, M. W. Preparation, Characterization and In Vivo Assessment of Gd-albumin and Gd-dendrimer Conjugates as Intravascular Contrast-Enhancing Agents for MRI. *J. Inorg. Biochem.* **2011**, *105*, 722−727.
(24) He, L.; Feng, L.; Cheng, L.; Liu, Y.; Li, Z.; Peng, R.; Li, Y.; Guo, L.; Liu, Z. Multilayer Dual-Polymer-Coated Upconversion Nanoparticles for Multimodal Imaging and Serum-Enhanced Gene Delivery. *ACS Appl. Mater. Interfaces* **2013**, *5*, 10381−10388.
(25) Yang, Y.-Y.; Wang, X.; Hu, Y.; Hu, H.; Wu, D.-C.; Xu, F.-J. Bioreducible POSS-Cored Star-Shaped Polycation for Efficient Gene Delivery. *ACS Appl. Mater. Interfaces* **2013**, *6*, 1044−1052.
(26) Zhu, Y.; Tang, G.-P.; Xu, F.-J. Efficient Poly(N-3-hydroxypropyl)aspartamide-Based Carriers via ATRP for Gene Delivery. *ACS Appl. Mater. Interfaces* **2013**, *5*, 1840−1848.
(27) Subramani, C.; Ofir, Y.; Patra, D.; Jordan, B. J.; Moran, I. W.; Park, M.-H.; Carter, K. R.; Rotello, V. M. Nanoimprinted Polyethyleneimine: A Multimodal Template for Nanoparticle Assembly and Immobilization. *Adv. Funct. Mater.* **2009**, *19*, 2937−2942.
(28) Cai, H.; An, X.; Cui, J.; Li, J.; Wen, S.; Li, K.; Shen, M.; Zheng, L.; Zhang, G.; Shi, X. Facile Hydrothermal Synthesis and Surface Functionalization of Polyethyleneimine-Coated Iron Oxide Nanoparticles for Biomedical Applications. *ACS Appl. Mater. Interfaces* **2013**, *5*, 1722−1731.
(29) Hunter, A. C. Molecular Hurdles in Polyfectin Design and Mechanistic Background to Polycation Induced Cytotoxicity. *Adv. Drug Delivery Rev.* **2006**, *58*, 1523−1531.
(30) Wagner, E.; Kloeckner, J. Gene Delivery Using Polymer Therapeutics. *Adv. Polym. Sci.* **2006**, *192*, 135−173.
(31) Nimesh, S.; Aggarwal, A.; Kumar, P.; Singh, Y.; Gupta, K. C.; Chandra, R. Influence of Acyl Chain Length on Transfection Mediated by Acylated PEI Nanoparticles. *Int. J. Pharm.* **2007**, *337*, 265−274.
(32) Petersen, H.; Fechner, P. M.; Fischer, D.; Kissel, T. Synthesis, Characterization, and Biocompatibility of Polyethylenimine-graft-poly(ethylene glycol) Block Copolymers. *Macromolecules* **2002**, *35*, 6867−6874.
(33) Aravindan, L.; Bicknell, K. A.; Brooks, G.; Khutoryanskiy, V. V.; Williams, A. C. Effect of Acyl Chain Length on Transfection Efficiency and Toxicity of Polyethylenimine. *Int. J. Pharm.* **2009**, *378*, 201−210.
(34) Liu, C.; Liu, F.; Feng, L.; Li, M.; Zhang, J.; Zhang, N. The Targeted Co-delivery of DNA and Doxorubicin to Tumor Cells via Multifunctional PEI-PEG Based Nanoparticles. *Biomaterials* **2013**, *34*, 2547−2564.
(35) Shi, S.; Shi, K.; Tan, L.; Qu, Y.; Shen, G.; Chu, B.; Zhang, S.; Su, X.; Li, X.; Wei, Y.; Qian, Z. The Use of Cationic MPEG-PCL-g-PEI Micelles for Co-delivery of Msurvivin T34A Gene and Doxorubicin. *Biomaterials* **2014**, *35*, 4536−4547.
(36) Wen, S.; Zhao, Q.; An, X.; Zhu, J.; Hou, W.; Li, K.; Huang, Y.; Shen, M.; Zhu, W.; Shi, X. Multifunctional PEGylated Multiwalled Carbon Nanotubes for Enhanced Blood Pool and Tumor MR Imaging. *Adv. Healthcare Mater.* [Online Early Access] DOI: 10.1002/adhm.201300631; Accessed 26th February **2014**.
(37) Wu, H.; Liu, G.; Wang, X.; Zhang, J.; Chen, Y.; Shi, J.; Yang, H.; Hu, H.; Yang, S. Solvothermal Synthesis of Cobalt Ferrite Nanoparticles Loaded on Multiwalled Carbon Nanotubes for Magnetic Resonance Imaging and Drug Delivery. *Acta Biomater.* **2011**, *7*, 3496−3504.
(38) Wen, S.; Zheng, F.; Shen, M.; Shi, X. Surface Modification and PEGylation of Branched Polyethyleneimine for Improved Biocompatibility. *J. Appl. Polym. Sci.* **2013**, *128*, 3807−3813.
(39) Jokerst, J. V.; Lobovkina, T.; Zare, R. N.; Gambhir, S. S. Nanoparticle PEGylation for Imaging and Therapy. *Nanomedicine* **2011**, *6*, 715−728.
(40) Roberts, M.; Bentley, M.; Harris, J. Chemistry for Peptide and Protein PEGylation. *Adv. Drug Delivery Rev.* **2012**, *64*, 116−127.
(41) Zhu, S.; Hong, M.; Tang, G.; Qian, L.; Lin, J.; Jiang, Y.; Pei, Y. Partly PEGylated Polyamidoamine Dendrimer for Tumor-Selective Targeting of Doxorubicin: The Effects of PEGylation Degree and Drug Conjugation Style. *Biomaterials* **2010**, *31*, 1360−1371.
(42) Cheng, Z.; Thorek, D. L. J.; Tsourkas, A. Gadolinium-Conjugated Dendrimer Nanoclusters as a Tumor-Targeted T1Magnetic Resonance Imaging Contrast Agent. *Angew. Chem., Int. Ed.* **2010**, *49*, 346−350.
(43) Huang, C.-H.; Nwe, K.; Al Zaki, A.; Brechbiel, M. W.; Tsourkas, A. Biodegradable Polydisulfide Dendrimer Nanoclusters as MRI Contrast Agents. *ACS Nano* **2012**, *6*, 9416−9424.
(44) Liu, Z.; Davis, C.; Cai, W.; He, L.; Chen, X.; Dai, H. Circulation and Long-term Fate of Functionalized, Biocompatible Single-Walled Carbon Nanotubes in Mice Probed by Raman Spectroscopy. *Proc. Natl. Acad. Sci. U. S. A.* **2008**, *105*, 1410−1415.
(45) Kim, B. H.; Lee, N.; Kim, H.; An, K.; Park, Y. I.; Choi, Y.; Shin, K.; Lee, Y.; Kwon, S. G.; Na, H. B.; Park, J.-G.; Ahn, T.-Y.; Kim, Y.-W.; Moon, W. K.; Choi, S. H.; Hyeon, T. Large-Scale Synthesis of Uniform and Extremely Small-Sized Iron Oxide Nanoparticles for High-Resolution T_1 Magnetic Resonance Imaging Contrast Agents. *J. Am. Chem. Soc.* **2011**, *133*, 12624−12631.
(46) Jung, K.-H.; Kim, H.-K.; Lee, G. H.; Kang, D.-S.; Park, J.-A.; Kim, K. M.; Chang, Y.; Kim, T.-J. Gd Complexes of Macrocyclic Diethylenetriaminepentaacetic Acid (DTPA) Biphenyl-2,2′-bisamides as Strong Blood-Pool Magnetic Resonance Imaging Contrast Agents. *J. Med. Chem.* **2011**, *54*, 5385−5394.
(47) Jansen, C. H. P.; Perera, D.; Makowski, M. R.; Wiethoff, A. J.; Phinikaridou, A.; Razavi, R. M.; Marber, M. S.; Greil, G. F.; Nagel, E.; Maintz, D.; Redwood, S.; Botnar, R. M. Detection of Intracoronary Thrombus by Magnetic Resonance Imaging in Patients With Acute Myocardial Infarction. *Circulation* **2011**, *124*, 416−424.
(48) Hadizadeh, D. R.; Kukuk, G. M.; Fahlenkamp, U. L.; Pressacco, J.; Schäfer, C.; Rabe, E.; Koscielny, A.; Verrel, F.; Schild, H. H.; Willinek, W. A. Simultaneous MR Arteriography and Venography with Blood Pool Contrast Agent Detects Deep Venous Thrombosis in Suspected Arterial Disease. *Am. J. Roentgenol.* **2012**, *198*, 1188−1195.
(49) Underhill, H. R.; Hatsukami, T. S.; Fayad, Z. A.; Fuster, V.; Yuan, C. MRI of Carotid Atherosclerosis: Clinical Implications and Future Directions. *Nat. Rev. Cardiol.* **2010**, *7*, 165−173.
(50) Oostendorp, M.; Douma, K.; Wagenaar, A.; Slenter, J. M. G. M.; Hackeng, T. M.; van Zandvoort, M. A. M. J.; Post, M. J.; Backes, W. H. Molecular Magnetic Resonance Imaging of Myocardial Angiogenesis After Acute Myocardial Infarction. *Circulation* **2010**, *121*, 775−783.
(51) Fink, C.; Ley, S.; Puderbach, M.; Plathow, C.; Bock, M.; Kauczor, H.-U. 3D Pulmonary Perfusion MRI and MR Angiography of Pulmonary Embolism in Pigs After a Single Injection of a Blood Pool MR Contrast Agent. *Eur. J. Radiol.* **2004**, *14*, 1291−1296.
(52) Inoue, T.; Kozawa, E.; Okada, H.; Inukai, K.; Watanabe, S.; Kikuta, T.; Watanabe, Y.; Takenaka, T.; Katayama, S.; Tanaka, J.; Suzuki, H. Noninvasive Evaluation of Kidney Hypoxia and Fibrosis Using Magnetic Resonance Imaging. *J. Am. Soc. Nephrol.* **2011**, *22*, 1429−1434.
(53) Cai, J.-M.; Hatsukami, T. S.; Ferguson, M. S.; Small, R.; Polissar, N. L.; Yuan, C. Classification of Human Carotid Atherosclerotic Lesions With In Vivo Multicontrast Magnetic Resonance Imaging. *Circulation* **2002**, *106*, 1368−1373.
(54) Brix, G.; Griebel, J.; Kiessling, F.; Wenz, F. Tracer Kinetic Modelling of Tumour Angiogenesis Based on Dynamic Contrast-enhanced CT and MRI Measurements. *Eur. J. Nucl. Med. Mol. Imaging* **2010**, *37*, 30−51.
(55) Bjørnerud, A.; Johansson, L. The Utility of Superparamagnetic Contrast Agents in MRI: Theoretical Consideration and Applications in the Cardiovascular System. *NMR Biomed.* **2004**, *17*, 465−477.
(56) Chou, S.; Shau, Y.; Wu, P.; Yang, Y.; Shieh, D.; Chen, C. In Vitro and In Vivo Studies of FePt Nanoparticles for Dual Modal CT/MRI Molecular Imaging. *J. Am. Chem. Soc.* **2010**, *132*, 13270−13278.
(57) Yang, K.; Gong, H.; Shi, X.; Wan, J.; Zhang, Y.; Liu, Z. In Vivo Biodistribution and Toxicology of Functionalized Nano-graphene Oxide in Mice after Oral and Intraperitoneal Administration. *Biomaterials* **2013**, *34*, 2787−2795.

(58) Wu, H.; Liu, G.; Zhuang, Y.; Wu, D.; Zhang, H.; Yang, H.; Hu, H.; Yang, S. The Behavior after Intravenous Injection in Mice of Multiwalled Carbon Nanotube/Fe_3O_4 Hybrid MRI Contrast Agents. *Biomaterials* **2011**, *32*, 4867−4876.